Chapter 4

Development of Silver Nanoparticles using Quercetin for the Colorimetric Sensing of L-Cysteine

GRAPHICAL OVERVIEW OF THE CHAPTER

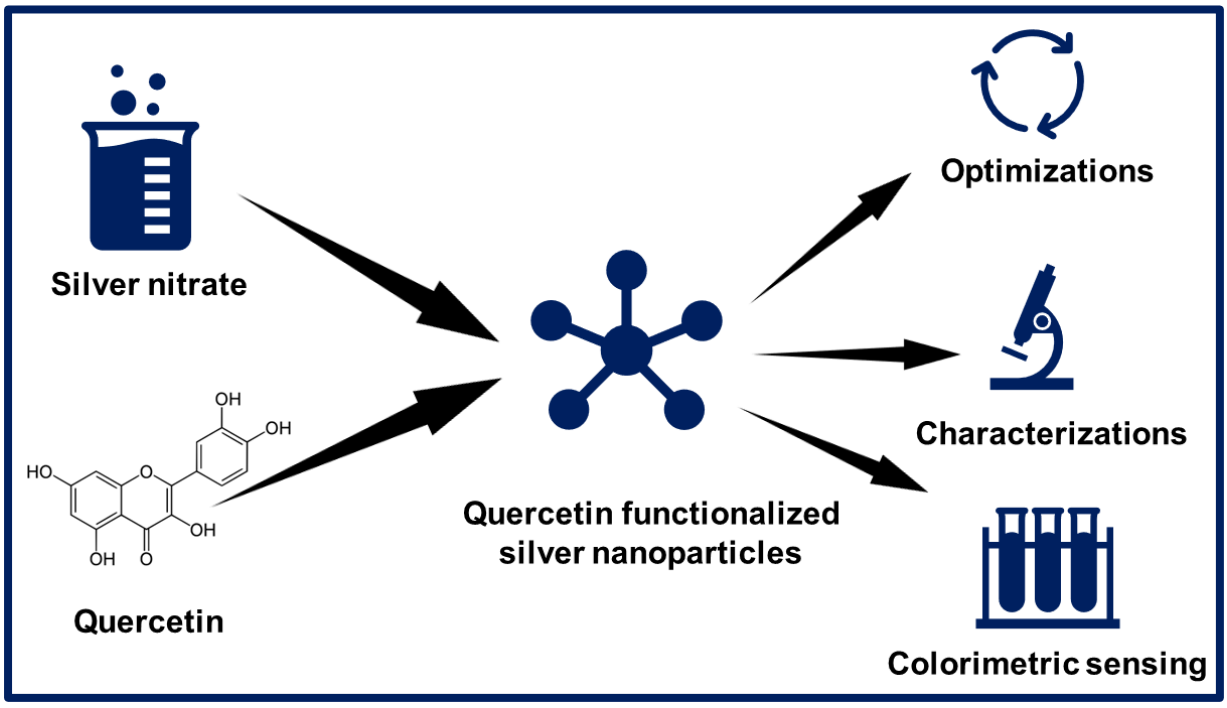

HIGHLIGHTS OF THE CHAPTER

- **Synthesis of quercetin functionalised silver nanoparticles (Q-AgNPs).**
- **Characterization of Q-AgNPs.**
- **Colorimetric sensing of L-Cys using Q-AgNPs.**
- **Selectivity analysis of Q-AgNPs for L-Cys detection.**
- **Sensitivity determination and analytical performance of Q-AgNPs for L-Cys detection.**

CHAPTER 4

DEVELOPMENT OF SILVER NANOPARTICLES USING QUERCETIN FOR THE COLORIMETRIC SENSING OF L-CYSTEINE

4.1 INTRODUCTION

Cysteine is a semi-essential amino acid for in preterm infants while non-essential amino acid in human adults and possess a thiol (-SH) group in its structure. As a result, it's often referred to as a sulfur-containing amino acid. Because it may be produced from other amino acids like methionine and serine, it is classified as semi-essential. Most high-protein foods and food products, such as chicken, turkey, yoghurt, cheese, eggs, sunflower seeds, and legumes are rich in cysteine [400]. It is commonly found as a cystine in proteins, where it forms a disulfide bond between two cysteine residues and is carefully preserved inside the protein to serve as a stabilizer for the proteins. Cysteine is a potent antioxidant with the ability to reduce reactive oxygen species (ROS), making it a promising antiaging agent [400]–[402]. It's found in keratin, which make up nails, toenails, skin, and hair. It also aids in collagen formation, which is necessary for skin suppleness and texture. Additionally, it protects liver parenchymal cells while simultaneously promoting hematopoietic activity, increasing leukocytes, and speeding up skin cell regeneration [403]. As a consequence, it can be said that cysteine plays an important role in activities such as protein production, metabolic functions, and detoxification processes.

Cysteine's intracellular concentration typically ranges from 20 to 200 µg. However, cysteine concentration in the plasma ranges from 13 to 60 µM while in the urine its acceptable concentration is <250 mg/L [404]–[408]. Literature studies shows that cells require cysteine in optimum concentration for normal functioning. The increased and decreased level of cysteine is generally found to be associated with number of disorders. High levels of cystine and cysteine in urine (>400 mg l^{-1}) indicate hepatic cystinuria and a few other disorders [409]. The concentration of cysteine has also been reported to elevate in the urine sample of patients having type 2 diabetes [410]. Furthermore, neurotoxicity is also linked to high cysteine levels, which is a well-established biomarker for a variety of metabolic diseases and illnesses. The decreased level of cysteine has been observed to be associated with problems like retarded growth, edoema, loss of hair pigments, damage to the skin, liver damages, drowsiness, body weakness,

leucocyte shortage, decreased haematopoiesis, psoriasis, neurological illnesses like Alzheimer's and Parkinson's diseases, and obesity [411]–[413]. There are also some reports showing that level of cysteine also gets fluctuated during microbial infection. Pathogenic microbe requires more cysteine for various metabolic functions. Hence level of cysteine gets decreased in the body [414]–[416]. The decreased level of cysteine can be used as marker for determination of microbial infection. For the selective detection of cysteine, significant effort has gone into developing analytical methods such as UV-vis spectrophotometry [417], fluorescence spectroscopy [418], high pressure liquid chromatography [419], immunoassay [420], gas chromatography [421], capillary electrophoresis [422], mass spectrometry [423], and electrochemical [424]. These present approaches have strong selectivity and sensitivity, but they have drawbacks such as time, expense, a laborious sample preparation procedures, specialised personnel, and complex equipment.

Because of the peculiar optical, physico-chemical, and magnetic characteristics of nano sized particles, nanotechnology appears to solve these difficulties to some extent. Bioremediation (biological pollutants, metal pollutants, and drug moieties), cosmetics, medications, medical devices, biosensors, and renewable energy are just a few of the domains where nanoparticles have been extensively investigated [425], [426]. Metal nanoparticles, meantime, have drawn a lot of interest due to their ease of use and remarkable sensitivity. Additionally, metal nanoparticles also have significant surface plasmon resonance (SPR) and a high extinction coefficient, making them a promising biosensing technique [427]–[431]. Silver nanoparticles have attracted a lot of attention among metallic nanoparticles because of their extraordinary extinction coefficient, high stability, and SPR [432], [433]. A number of approaches have been described to manufacture silver nanoparticles to improve biocompatibility and sensitivity for biomedical applications, including micro-emulsion methods, sol-gel methods, solution evaporation methods, microwave-assisted methods, and co-precipitation methods [434], [435]. Green synthesis technologies, which reduce the usage of harmful and unpleasant substances and instead use naturally occurring metabolites as reducing and capping agents, have emerged as an alternative method for the synthesis of nanoparticles. These naturally occurring compounds are often non-toxic, biocompatible, and inexpensive.

Quercetin is a natural pigment found in plants also known as plant-flavonoid. It may be found in a variety of foods and plants, including red wine, onions, berries. apples, and green tea. It possesses anti-inflammatory and antioxidant properties that may help decrease edoema, destroy cancer cells, regulate blood sugar, and prevent heart diseases [436]–[438]. The purpose

of current work was to produce silver nanoparticles functionalized by quercetin (Q-AgNPs) through one pot synthesis process. The Q-AgNPs were characterized by various analytical and microscopic techniques. The Q-AgNPs developed were intended for use in a colorimetric procedure that would reliably, easily, and quickly identify L-Cys in water and other complicated fluids including urine and foetal bovine serum.

4.2 MATERIALS AND METHODS

4.2.1 Chemicals

All the glassware's used in the study were made up of borosilicate (Borosil, India). Glassware's were properly washed, rinsed and dried before using in the study. Merck, India, provided the chemicals like L-Cys, quercetin, silver nitrate, and ethanol. Hi-Media (India) provided the sodium hydroxide. Sisco Research Laboratories Pvt. Ltd., India, provided the amino acids viz. L-Tyr, L-Lys, L-Asn, L-Ala, L-Gln, L-Asp, L-Phe, L-Val, L-Leu, L-His, and L-Met. Thermo Fisher, India, provided the foetal bovine serum (FBS). A healthy male of the institution volunteered to give a urine sample. The urine sample for the study was taken with the consent of a volunteer at the institution's medical facility with ethical permission from institutes ethical committee (IEC/Project No-01/2022). The Milli Q water (18.2 mΩ) for the study was from the institution's assembly (Merck Millipore).

4.2.2 Q-AgNPs synthesis and optimization

The synthesis of Q-AgNPs was done using aqueous solution of silver nitrate (2 mM) and quercetin (50 µM). The 50 µM quercetin solution was prepared by dilution with water from stock solution of quercetin (1 mM in 80 % ethanol). The amount of quercetin (volume) was varied from 0.062 – 1.5 mL against constant silver nitrate i.e., 5 mL volume to optimize ratio (volume/volume) for optimal synthesis. The pH of quercetin mixture was also varied from 4-11 to achieve optimal synthesis of Q-AgNPs. The contents of the reaction were incubated in dark at 30 °C for synthesis. Results were monitored through UV-vis spectroscopy. Furthermore, we also investigated the stability of synthesized Q-AgNPs at various temperatures (10 °C to 90 °C), pH (2 to 10) and in electrolytes (NaCl 0.89 % and KCl 3.5 mM).

4.2.3 Q-AgNPs Characterizations

Q-AgNPs synthesized were further subjected to characterizations through various techniques. UV-vis spectroscopy of Q-AgNPs was done using spectrophotometer (Model Evolution 201, Thermo Scientific, India) from 300 – 800 nm to confirm synthesis and to determine absorption maxima. XRD of produced Q-AgNPs was done in order to determine their crystal structure (10 – 90° 2θ angle). The shape and size of Q-AgNPs was determined using FESEM (Carl Zeiss SMT AG, Germany) and TEM microscopy (Electron microscope, JEM 1400, JEOL, USA). The functional groups present on Q-AgNPs were analyzed using FTIR spectroscopy (Bruker, Germany) from 4000 – 400 cm^{-1}. Furthermore, dynamic light scattering of Q-AgNPs was also done to determine their size (hydrodynamic) and zeta potential using Malvern Zeta-sizer equipment.

4.2.4 Detection of L-Cys using Q-AgNPs

L-Cys was detected simply by mixing it with Q-AgNPs followed by incubation. The protocol briefly involves addition of 500 µl of Q-AgNPs to a 1.5 mL microcentrifuge tube followed by addition of 485 µl of Milli Q water and mixing by inverting the microcentrifuge tube. Following that, 15 µl L-Cys of 1 mM concentration was incorporated to the aforesaid reaction and stirred thoroughly. The contents were allowed to react for 15 min at 55 °C. A control system lacking L-Cys was also incubated at the same time. The variations were seen visually and UV-vis spectrophotometrically from 300 to 800 nm after incubation.

4.2.5 Determination of Q-AgNPs selectivity for L-Cys

Selectivity is an absolute requirement since it defines the scope of the sensor in evaluation and monitoring. The Q-AgNPs were treated against L-Cys and other amino acids viz. L-Tyr, L-Lys, L-Asn, L-Ala, L-Gln, L-Asp, L-Phe, L-Val, L-Leu, L-His, and L-Met to determine its selectivity as per protocol mentioned in section 4.2.4. All other amino acids were used at the same concentration as L-Cys. Visual and UV-vis spectrophotometric measurements were used to determine the changes occurred.

4.2.6 Evaluation of temperature and time effect on the detection of L-Cys

In colorimetric biosensing, reaction time and temperature are also very critical. Employing Q-AgNPs, we explored the influence of time and temperature on L-Cys detection in this experiment. We altered the incubation temperature from 25 to 75 °C to see how temperature

affected the results. Similarly, the duration of incubation was changed from 0 to 45 min to investigate the influence of time on detection of L-Cys. In both cases, the alterations were observed with the naked eye and with UV-vis spectrophotometry.

4.2.7 Analysis of Q-AgNPs performance in aqueous, urine and FBS solution for the L-Cys detection

In biosensors, strong analytical performance is typically required, therefore the efficiency of the biosensor was tested in L-Cys-containing aqueous, urine, and FBS solutions to examine the realistic capability of Q-AgNPs for recognizing L-Cys. The efficiency of Q-AgNPs in L-Cys-containing aqueous and FBS solutions was measured in the range of 0-15 µM, while the L-Cys concentration in urine samples was measured in the range of 0-20 µM. UV-vis spectrophotometry and ocular observation were used to keep track of the findings. The following formula was used to calculate the limit of detection (LOD) and limit of quantification (LOQ):

$$\mathbf{LOD} = \frac{3.3 * \text{Standard deviation of lowest concentration}}{\text{Slope of Calibration line}}$$

$$\mathbf{LOQ} = \frac{10 * \text{Standard deviation of lowest concentration}}{\text{Slope of Calibration line}}$$

4.3 RESULTS AND DISCUSSION

4.3.1 Synthesis and optimization

The synthesis of Q-AgNPs was done through single step (one-pot) synthesis approach. The colorless silver nitrate solution was mixed with quercetin solution for about 5 h in dark conditions. After incubation the colour of the solution was appeared to be yellow. The yellow appearance initially hints the Q-AgNPs synthesis. The UV-vis spectroscopy was used to confirm the synthesis of Q-AgNPs. UV-vis spectrum of Q-AgNPs highlighted an absorption peak at 418 nm (Figure 4.1). The finding was supported by literature showing that silver nanoparticles exhibit absorption band around 400 nm [439], [440]. Existing literature also shows that a single absorption peak is also indicative of spherical shape silver nanoparticles [435]. The mechanism of Q-AgNPs synthesis involves reduction of Ag^{+} ions into Ag^{0} using the hydroxyl (-OH) groups of quercetin [441]. FTIR analysis revealed that quercetin exhibited phenolic bending at 1380 cm^{-1}, and same was missing case of Q-AgNPs (Figure 4.5), indicating

their involvement in Q-AgNPs synthesis [442]–[444]. Many previous studies have revealed the involvement of hydroxyl groups (-OH) in the reduction of silver and gold ions to produce nanoparticles [445]–[447]. The cinnamyl group in present in the quercetin's chemical structure displayed a peak at 374 nm in UV-visible spectrum (Figure 4.1) [448]. However, the UV-vis spectrum of $AgNO_3$ doesn't show any absorption peak.

The optimization results for $AgNO_3$: quercetin ratio (volume by volume) revealed that 5:1 ratio was optimum for the synthesis as beyond this ratio there was disturbance in the UV-vis absorption spectrum (Figure4.2). Similarly, the pH 10 was found to be optimum for Q-AgNPs synthesis (Figure 4.3).

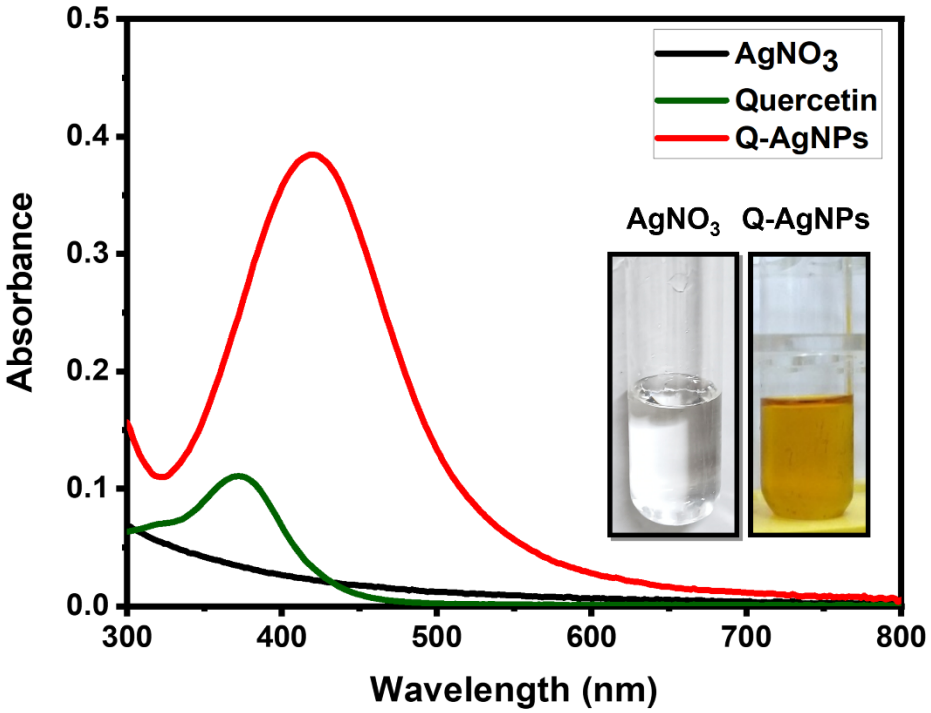

Figure 4.1: UV-vis spectrum of silver nitrate, quercetin and Q-AgNPs (dilution factor 2.5), inset colour of synthesized Q-AgNPs.

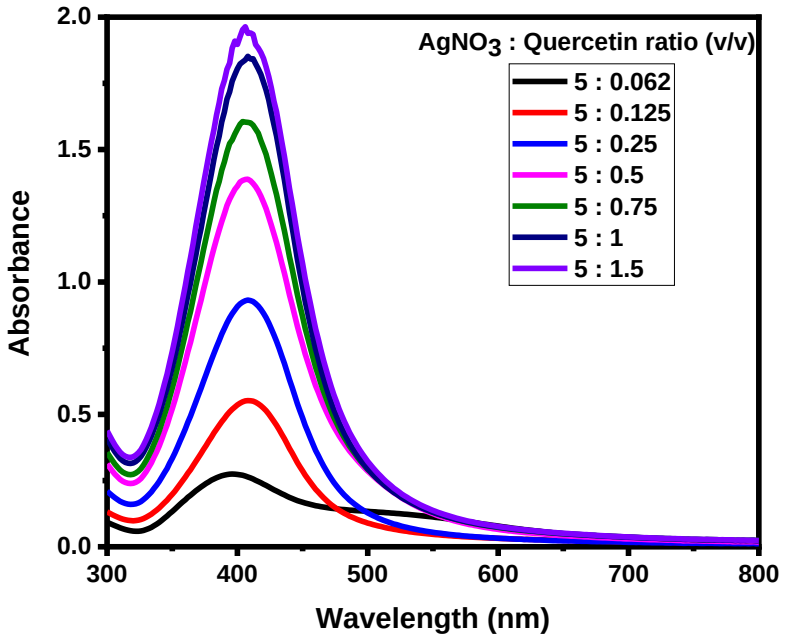

Figure 4.2: Effect of various amounts of quercetin (volume/volume) on Q-AgNPs synthesis.

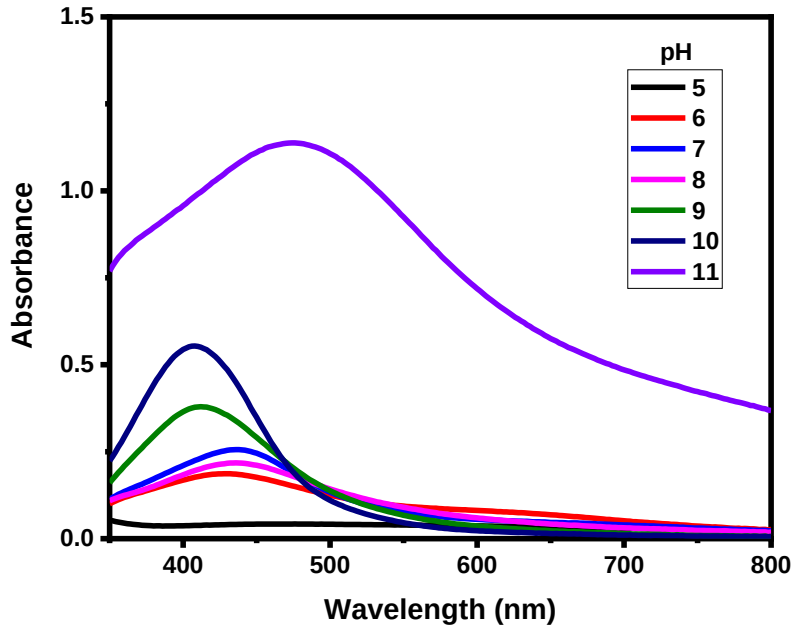

Figure 4.3: Effect of various pH conditions on the Q-AgNPs synthesis (dilution factor 2.5).

4.3.2 Analysis of Q-AgNPs stability

The results of storage stability (4 °C) displayed that Q-AgNPs were enough stable for 60 days (Figure 4.4a). The stability of Q-AgNPs was also determined at various pH conditions. UV-vis spectroscopy results show that Q-AgNPs retains their stability from pH 6.5 to pH 8.0 as there

was no substantial shifts in the spectrum of Q-AgNPs absorption band in this pH range. Additionally, significant changes in the spectrums of Q-AgNPs were detected at acidic pH range (2-5) and alkaline pH (9-10), showing particle destabilization at extremely acidic and alkaline environments (Figure 4.4b). The Q-AgNPs stability was also tested in a variety of electrolytes and temperatures. UV-vis examination demonstrated that Q-AgNPs were sufficiently stable in electrolytic solution of KCl and NaCl (Figure 4.4c). Q-AgNPs thermal stability research demonstrated that nanoparticles were stable up to 50 °C, but as we increased the temperature up to 90 °C, they began to lose stability (Figure 4.4d).

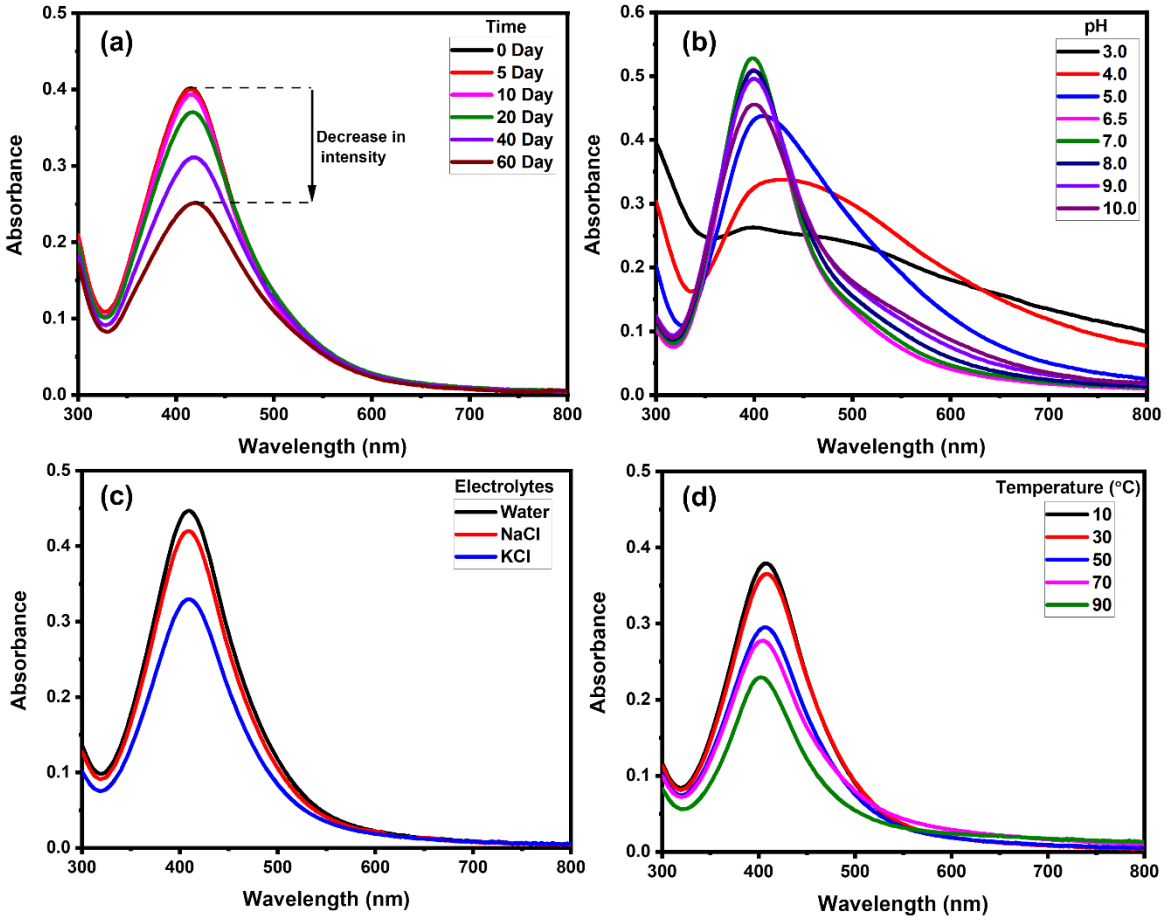

Figure 4.4: (a) The UV-vis spectrums of stored (4 °C) Q-AgNPs at various time, (b) Q-AgNPs UV-vis spectrums at various pH conditions, (c) Q-AgNPs UV-vis spectrums after treatment against various solvents, (d) Q-AgNPs UV-vis spectrums after treatment at various temperature.

4.3.3 Characterizations of Q-AgNPs

4.3.3.1 XRD analysis

XRD analysis of Q-AgNPs without and with L-Cys was done from 10-90° two theta angle. XRD pattern of Q-AgNPs with and without L-Cys displayed Bragg's reflections at 81.68°, 77.6°, 64.7°, 44.4°, and 38.36° and were corresponding to 222, 311, 220, 200, and 111 planes (Figure 4.5). The interplanar spacings were 1.224 Å, 1.436 Å, 1.955 Å, and 3.336 Å for the planes 222, 311, 220, 200, and 111 respectively. The results were in accordance to the standard silver values against JCPDS file number 04-0783 [449]. The findings revealed that Q-AgNPs have a crystalline structure that is maintained even when L-Cys is present.

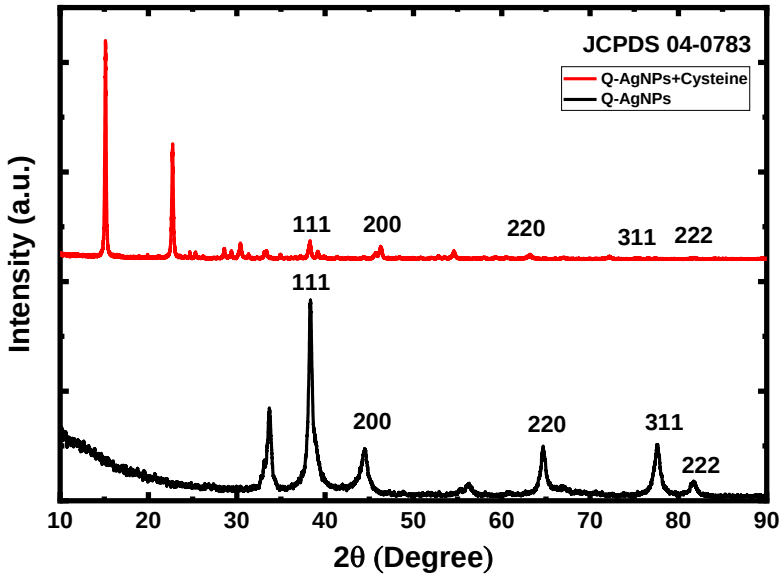

Figure 4.5: Q-AgNPs XRD patterns with and without L-Cys.

4.3.3.2 FTIR analysis

The functional groups of Q-AgNPs, quercetin, and silver nitrate ($AgNO_3$) were revealed through FTIR spectroscopy [450], [451]. This approach may also be used to identify the ligands bound to nanoparticles based on their vibrational fingerprints [451]. The FTIR spectrum of all the mentioned compounds were acquired from 4000-400 cm^{-1}. The details of functional groups identified by FTIR analysis has been listed in Table 4.1. In the FTIR spectrum of $AgNO_3$ the peak at 1290 cm^{-1} (Figure 4.6a) was believed to be due to the symmetrical stretching's of N=O functional group of $AgNO_3$ [452], [453]. The peak at 1661 cm^{-1} in the FTIR spectra of quercetin was due to carbonyl (C=O) group, whereas stretching of C=C aromatic ring were found at 1512,

1560, and 1614 cm^{-1} (Figure 4.6a). Phenolic group of quercetin displayed OH bending at 1380 cm^{-1}. Furthermore, results indicated that, C-H in aromatic hydrocarbons has an in-plane bending band at 1317 cm^{-1}, whereas peaks at 679, 820, and 1014 cm^{-1} were contributed by out-of-plane bending. The aryl ether ring C-O stretching, the phenolic C-O stretching, and the ketonic C-CO-C stretching and bending were found at 1261, 1199, and 1163 cm^{-1}, respectively. Peaks from 3270 to 3401 cm^{-1} were believed to be attributed by stretching's of -OH groups. The FTIR spectra of quercetin produced was found to be in close harmony with prior studies [442], [443]. The FTIR spectra of Q-AgNPs highlighted the peak at 1640 cm^{-1} as a result of carbonyl (C=O) stretching (Figure 4.6a). The appearance of a C=O peak in Q-AgNPs indicates that flavonoid molecules are present on the Q-AgNPs without destroying its native structure [454], [455]. Furthermore, the O-H stretching of Q-AgNPs was recorded from 3230 to 3365 cm^{-1}, contributed by OH groups of aqueous colloidal solution of Q-AgNPs [454]–[456]. The amplitude some of the other peaks in the Q-AgNPs FTIR spectrum was low, hence a magnified section from 1800-950 cm^{-1} has been highlighted in Figure 4.6b and description has been provided in Table 4.1. Therefore, it can be said that the FTIR spectrum of Q-AgNPs was in close proximity to those of quercetin.

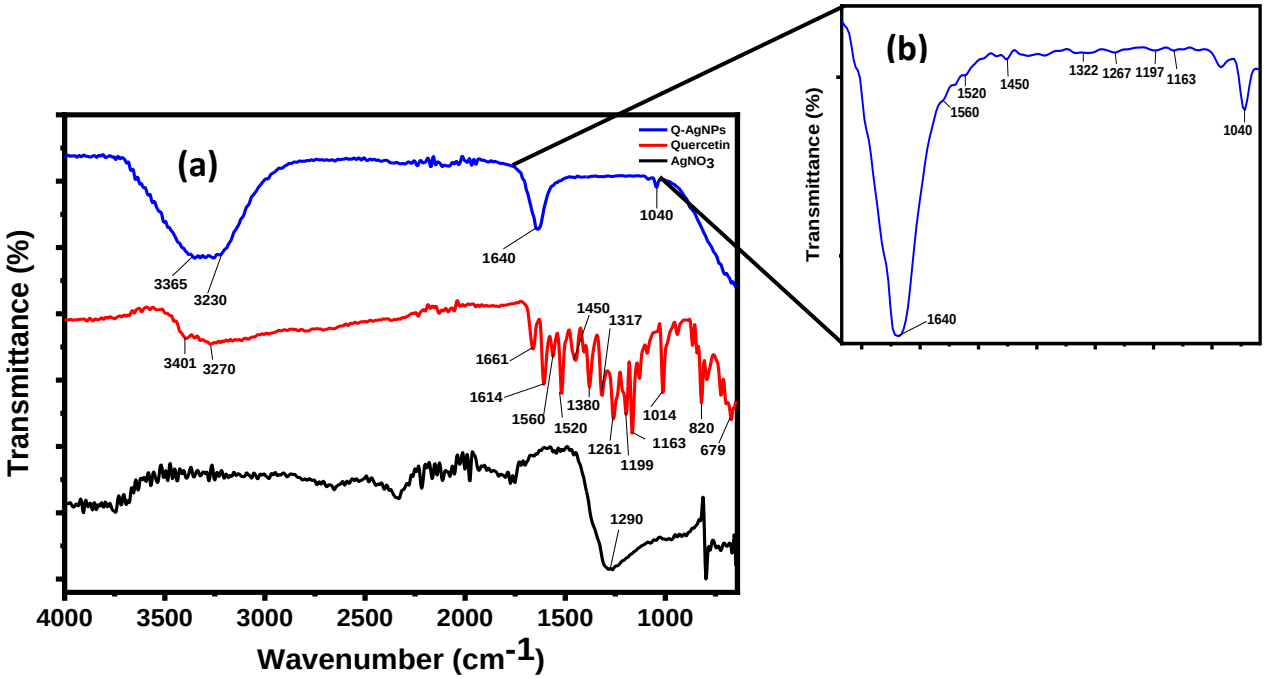

Figure 4.6: (a) FTIR spectrum of $AgNO_3$, quercetin, and Q-AgNPs, (b) Inset magnified region of Q-AgNPs from 1700-1000 cm^{-1}.

Table 4.1: Description of functional groups as revealed by FTIR analysis of silver nitrate, quercetin and Q-AgNPs

Compound	Functional group	Wavenumber (cm^{-1})
$AgNO_3$	Symmetrical stretching of N=O	1290
Quercetin	Carbonyl (C=O) group	1661
	C=C aromatic ring stretching	1512, 1560, and 1614
	OH bending	1380
	C-H in aromatic hydrocarbons in-plane bending	1317
	C-H in aromatic hydrocarbons out-of-plane bending	679, 820, and 1014
	Aryl ether ring C-O stretching	1261
	Phenolic C-O stretching	1199
	Ketonic C-CO-C stretching	1163
	Stretching of -OH groups	3270-3401
Q-AgNPs	Carbonyl (C=O) stretching	1640
	O-H stretching	3230-3365
	Aromatic ring stretches of the C=C	1520 and 1560
	C-H in-plane bending of aromatic hydrocarbons	1322
	C-H out-of-plane bending	1040
	Phenolic stretching	1267
	Aryl ether ring C-O stretching	1197
	Ketonic C-CO-C stretch and bending	1163

4.3.3.3 SEM, TEM, and DLS investigation of Q-AgNPs

The morphology and the size of synthesized Q-AgNPs was determined through techniques like TEM, SEM, and DLS. TEM and SEM are generally used to observe particle morphology and their size while DLS analysis predicts the hydrodynamic size of particles. Furthermore, these studies were also used for the better understanding of cysteine-induced aggregation of Q-AgNPs against control (Q-AgNPs without cysteine). The results of the study predicted that Q-AgNPs were approximately 40 nm in size (Figure 4.7a,c,e). The morphology of Q-AgNPs was

observed to be spherical (Figure 4.7a,c). Moreover, the Q-AgNPs sample having no L-Cys showed that particles were well disseminated, while there was aggregation in the Q-AgNPs sample with L-Cys (Figure 4.7b,d,f).

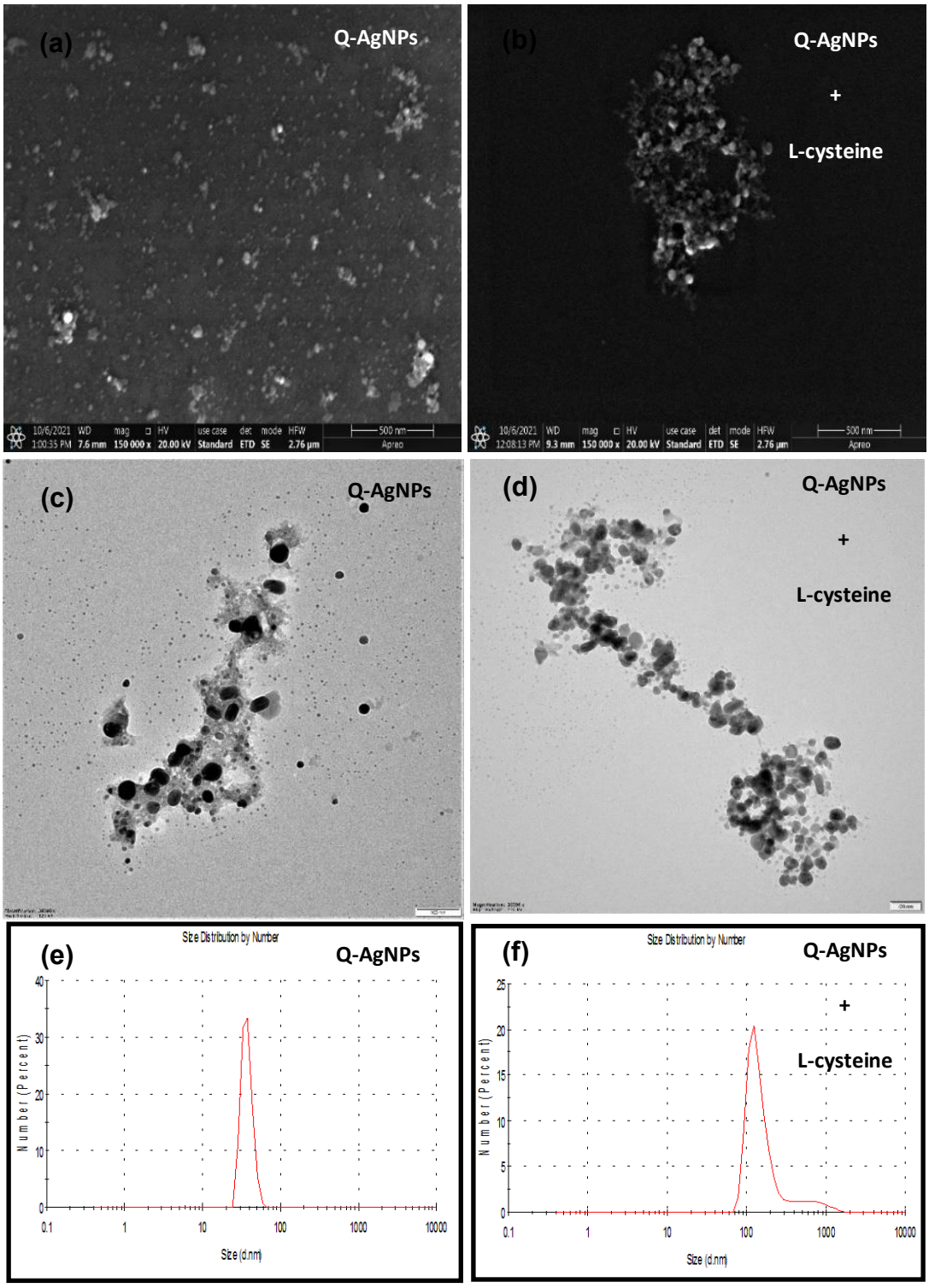

Figure 4.7: SEM images of Q-AgNPs (a) without L-Cys, (b) with L-Cys, TEM images of Q-AgNPs (c) without L-Cys, (d) with L-Cys, and DLS analysis of Q-AgNPs (e) without (f) with L-Cys.

4.3.4 L-Cys detection using Q-AgNPs and their mechanism of action

The detection of L-Cys was examined by monitoring visual and spectral changes in the Q-AgNPs solution with L-Cys and without L-Cys as control. The UV-vis spectrum results highlighted that control Q-AgNPs exhibited absorption maximum at 418 nm (Figure 4.8a) while in L-Cys incorporated Q-AgNPs it was found at 442 nm (Figure 4.8a). Thus, Q-AgNPs spectrum exhibited a red shift of 24 nm having L-Cys. Moreover, there was also significant variation in the colour of Q-AgNPs when treated with L-Cys. Control AgNPs visually appears to be yellowish in colour while test Q-AgNPs were brownish in appearance (Figure 4.8a inset). The mechanism of agglomeration may be the agglomeration of Q-AgNPs by the interaction between thiol (-SH) group of cysteine Ag of Q-AgNPs (Figure 4.8b). The cysteine thiol group has a high affinity for Ag [457], forming a solid Ag-S bond. Thus, the agglomeration of Q-AgNPs was believed to be caused by the widespread establishment of Ag-S bonds (Figure 4.8b). Previous studies have shown that cysteine may attach to the surface of silver nanoparticles by a strong Ag-S interaction, which is followed by agglomeration [451], [458], [459]. UV-vis spectrum of L-Cys containing Q-AgNPs highlighted the cysteine triggered agglomeration as indicated by a red shift and brown colour appearance from yellow. SEM and TEM investigation further verified the agglomeration of Q-AgNPs, with clustering of Q-AgNPs visible with the administration of L-Cys (Figure 4.7b,d) to that of control (Figure 4.7a,c). The agglomeration of Q-AgNPs due to L-Cys was further validated by hydrodynamic measurements of Q-AgNPs. DLS results shows that L-Cys promotes Q-AgNP agglomeration as the hydrodynamic size of Q-AgNPs was enhanced many times (Figure 4.7e,f).

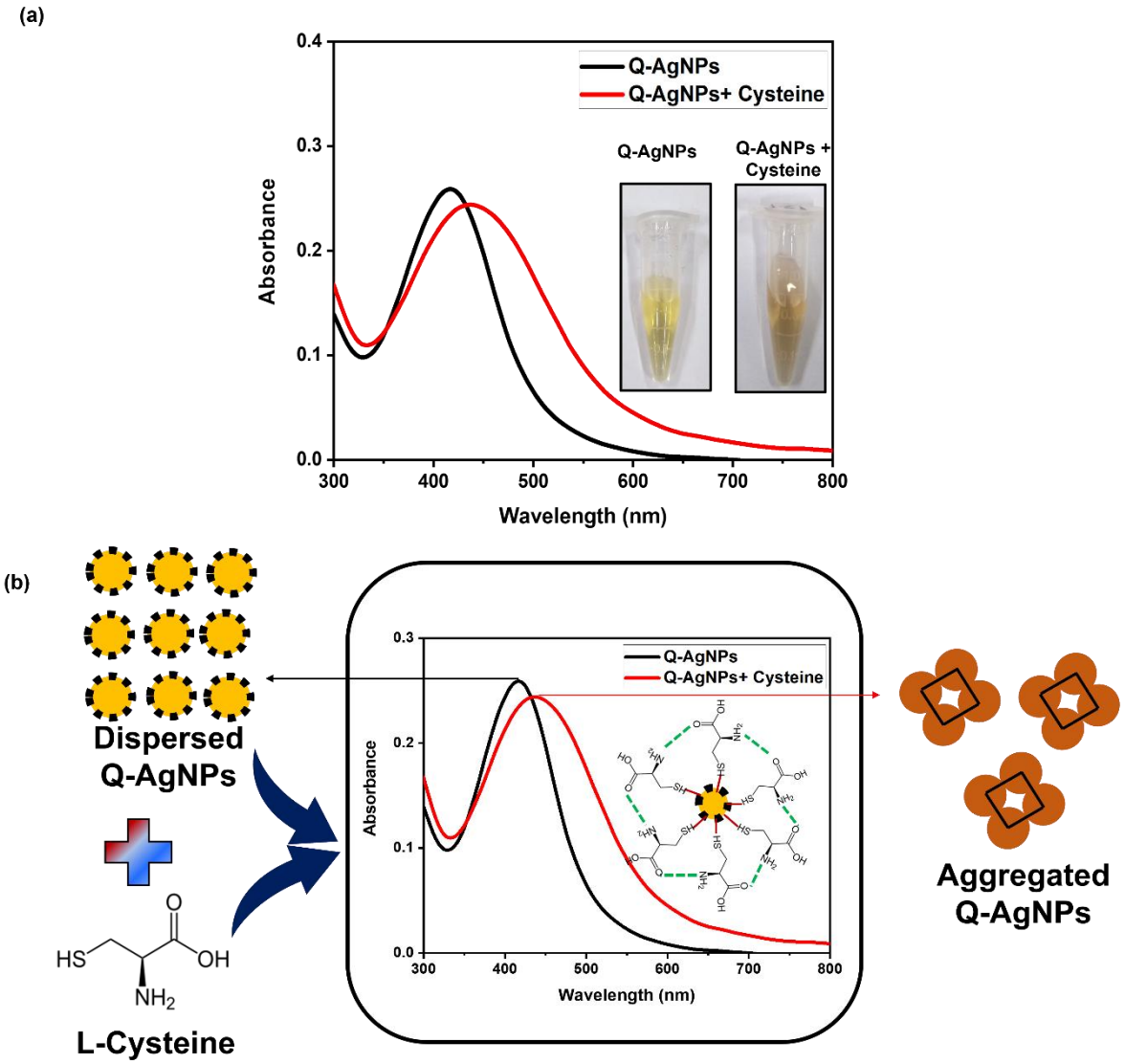

Figure 4.8: (a) Effects caused in the Q-AgNPs UV-visible spectrum with addition of L-Cys (red line) in comparison to control Q-AgNPs lacking L-Cys (black line), inset Q-AgNPs colour in presence and absence of L-Cys (b) A graphical illustration of the Q-AgNPs biosensing mechanism.

4.3.5 The influence of variable time and temperature on the L-Cys detection by Q-AgNPs

In attempt to improve the sensing, the influence of various temperatures was evaluated. Q-AgNPs having 15 µM L-Cys along with control Q-AgNPs devoid of L-Cys were incubated at variable temperature from 25 °C to 75 °C for a duration of 15 min. The results from UV-vis analysis (Figure 4.9a-f) indicated that the 24 nm highest red shift at 55 °C (Table 4.2), hence 55 °C temperature was selected for the rest of the investigation. Additionally, during evaluating the influence of time duration on biosensing at optimal temperature, we

noticed a substantial 8 nm red shift after just 5 min, which grew to 24 nm after 15 min (Figure 4.10). However, after 30 min, there's been fast agglomeration of Q-AgNPs (Figure 4.10).

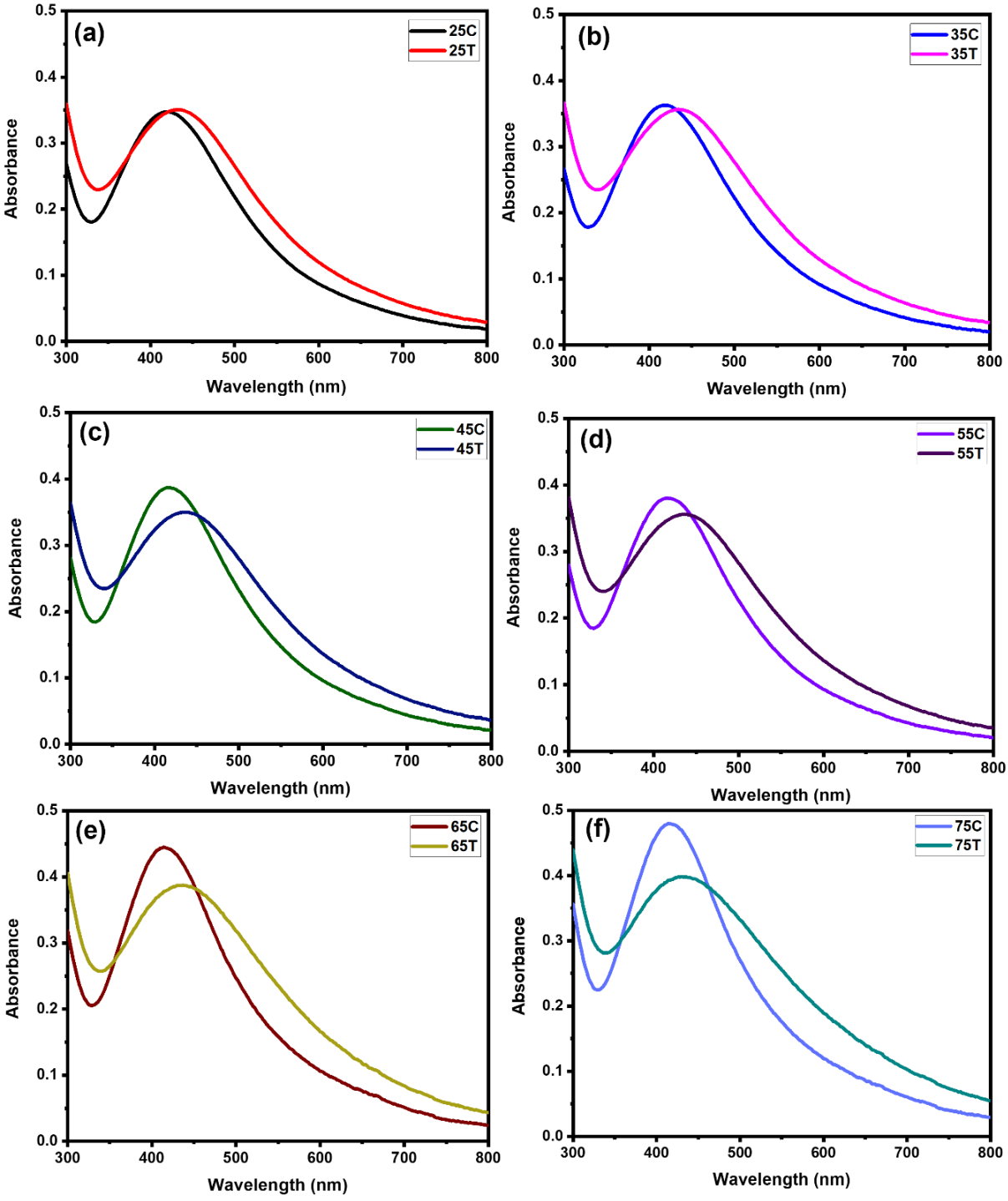

Figure 4.9: (a-f) Effects of varying temperatures on L-Cys sensing (*C corresponds to control (Q-AgNPs without L-Cys), while T corresponds to test (Q-AgNPs with cysteine)).

Table 4.2: Shifting in the wavelength of Q-AgNPs at varying temperature conditions.

Temperature (°C)	Shift in wavelength (nm)
25	13
35	16
45	19
55	24
65	18
75	17

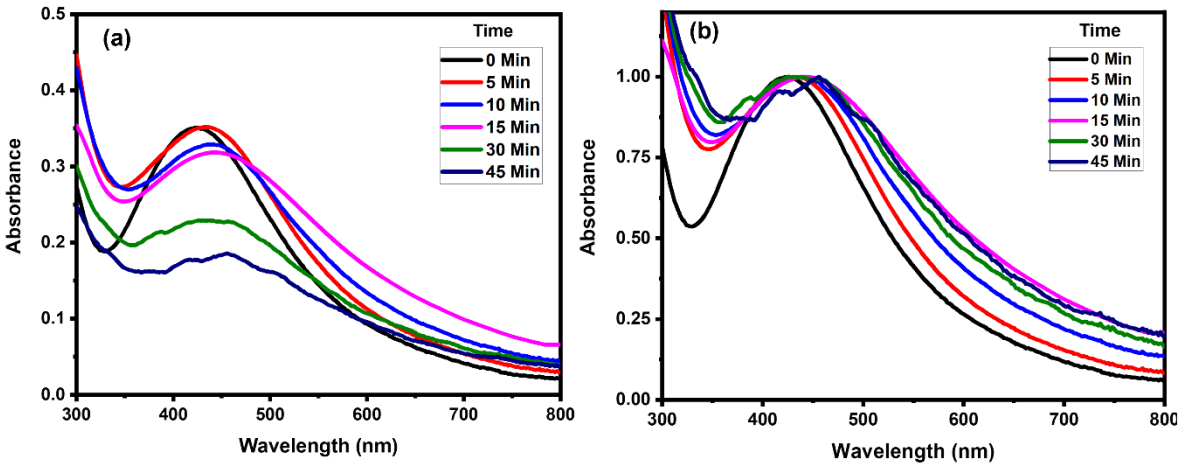

Figure 4 .10: (a) Variations in the UV-vis spectrum of Q-AgNPs at various time of sensing (b) Normalized UV-vis spectra of Q-AgNPs at various time of sensing.

4.3.6 Q-AgNPs selectivity towards L-Cys detection

The Q-AgNPs performance versus L-Tyr, L-Lys, L-Asn, L-Ala, L-Gln, L-Asp, L-Phe, L-Val, L-Leu, L-His, and L-Met was used to establish their selectivity towards L-Cys. The Q-AgNPs UV-vis spectrums treated with various amino acids demonstrate that only L-Cys containing Q-AgNPs have a noticeable red shift (Figure 4.11a). The cysteine-containing Q-AgNPs showed a considerable colour transformation when examined with the naked eye, however no such impact was seen with the other amino acids (Figure 4.11b). Visual observations corroborated the spectrophotometric findings that L-Cys preferentially reacts with Q-AgNPs and caused considerable tweaks. The interactions of Q-AgNPs with the free -SH group of L-Cys [57] was the most probable reason for the selectivity. All other amino acids lack the free -SH group. However, L-Met contains a thioether but does not take participate in bond formation [460].

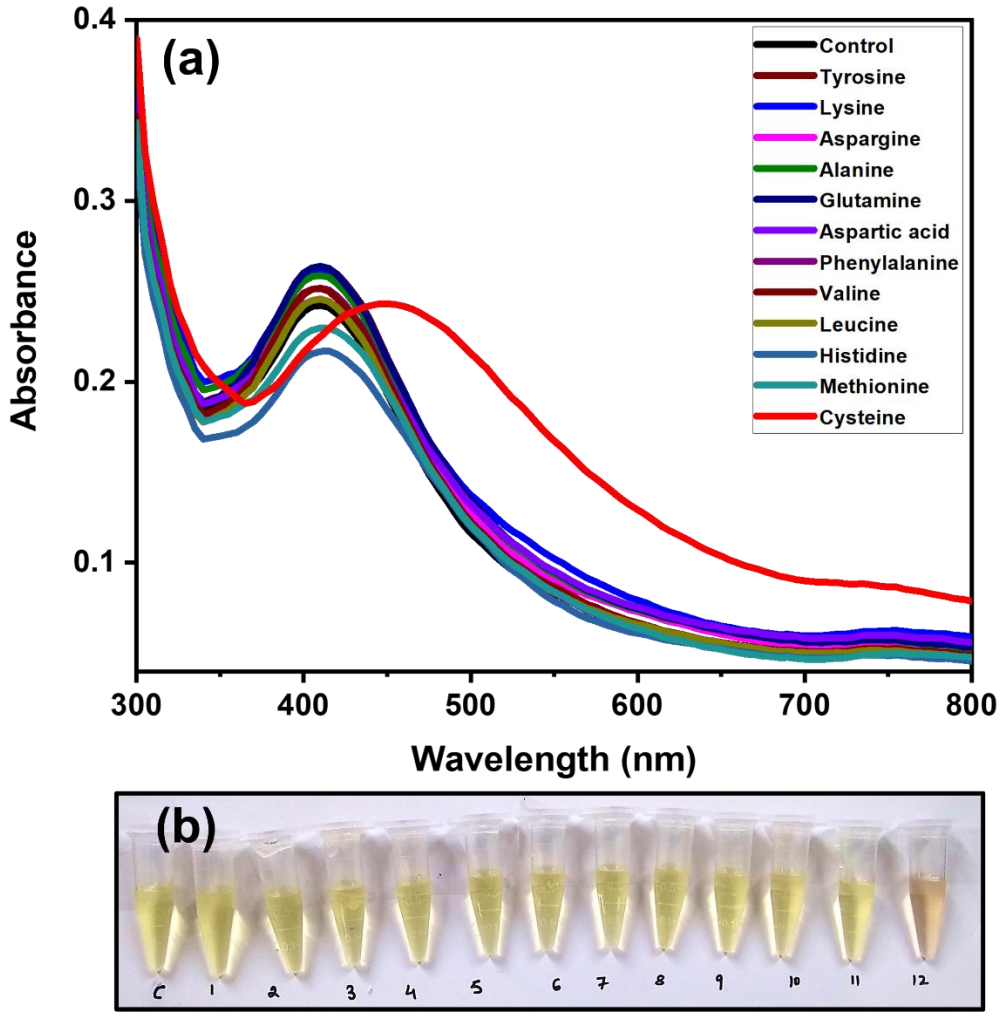

Figure 4.11: (a) Selectivity analysis of Q-AgNPs towards cysteine in contrast to other amino acids through UV-vis spectroscopy (b) Changes in Q-AgNPs colour against different amino acids*.

** C-control, 1: L-Tyr, 2: L-Lys, 3: L-Asn, 4: L-Ala, 5: L-Gln, 6: L-Asp, 7: L-Phe, 8: L-Val, 9: L-Leu, 10: L-His, 11: L-Met, and 12: L-Cys*

4.3.7 Analytical performance and sensitivity of Q-AgNPs for L-Cys detection

Q-AgNPs sensitivity towards L-Cys in water and complex biological samples (urine and FBS) was assessed using UV-vis spectral investigations and colorimetric observations. To reduce the matrix influence, dilution of urine and FBS samples were done 100 times by Milli Q water [461]. Various concentrations of L-Cys spiked solution of aqueous, urine, and FBS were added to Q-AgNPs as stated in the procedures section. UV-vis spectroscopy results indicated that the Q-AgNPs wavelength shown a red shift with increasing L-Cys concentration in aqueous solution from 0.25 to 15 µM (Figure 4.12a), with highest red shift of 24 nm at 15 µM L-Cys concentration. Q-AgNPs colour changed from yellow to brownish yellow was

observed as cysteine content increased (Figure 4.12c). The LOD for L-Cys in an aqueous solution was 21.1 nM, whereas the LOQ was found to be 63 nM, according to the linear regression equation (Figure 4.12b).

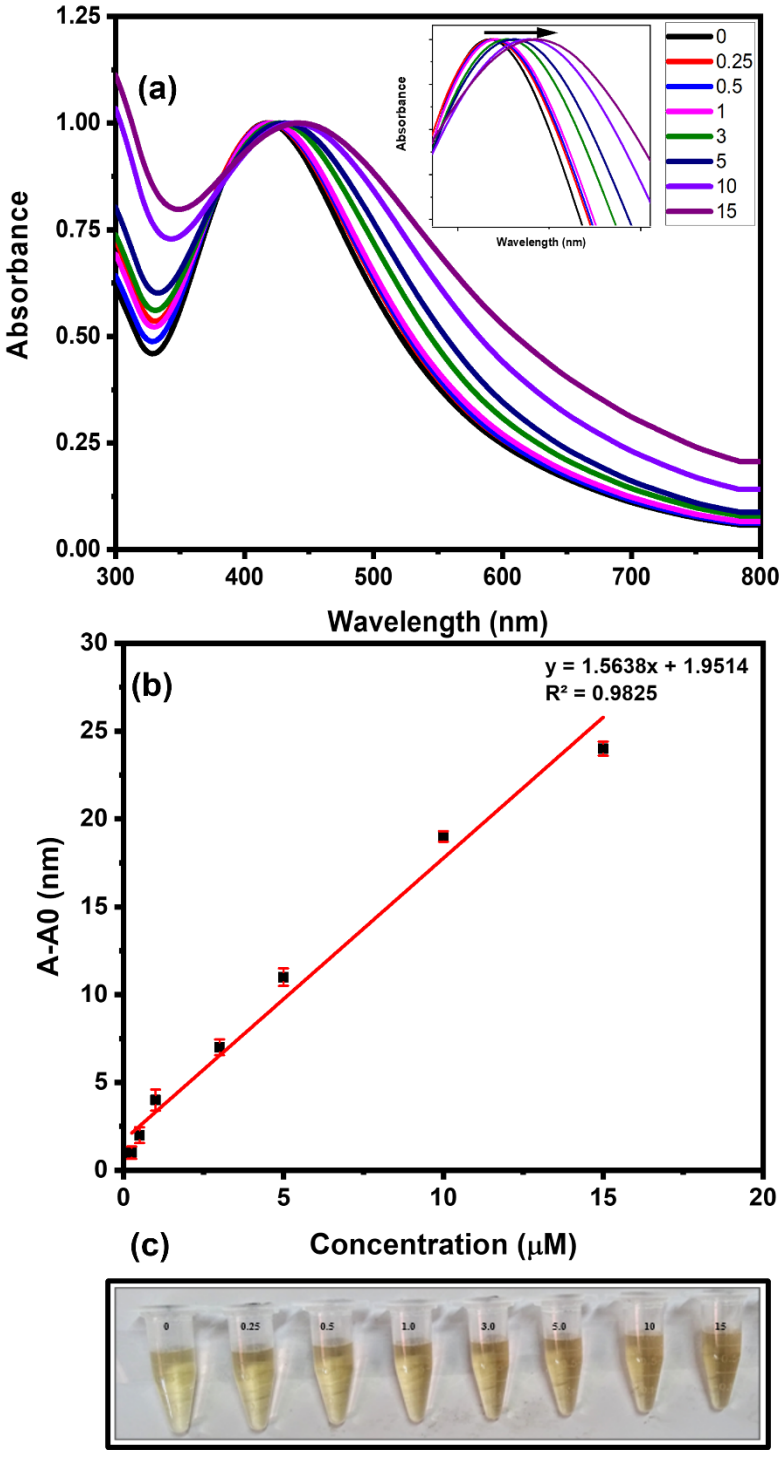

Figure 4.12: (a) UV-vis spectrum of Q-AgNPs at different aqueous concentration of L-Cys (0.25-15 µM) (normalized spectra), inset wavelength shifting (b) Regression line displaying a red shift with respective L-Cys concentration, (c) Colour change in Q-AgNPs at different L-Cys concentration in water sample.

Identical UV-visible spectral and visual trends in Q-AgNPs were noticed in the urine solution of L-Cys. With increasing cysteine content in urine samples (Figure 4.13a), there was increasing red shift, maximum red shift of 18 nm at 20 µM L-Cys concentration. The Q-AgNPs LOD for L-Cys in urine samples was 86 nM, whereas the LOQ was 260 nM, as established by regression equation (Figure 4.13b). Moreover, a colour change brownish yellow from yellow was also noticed increasing L-Cys content (Figure 4.13c).

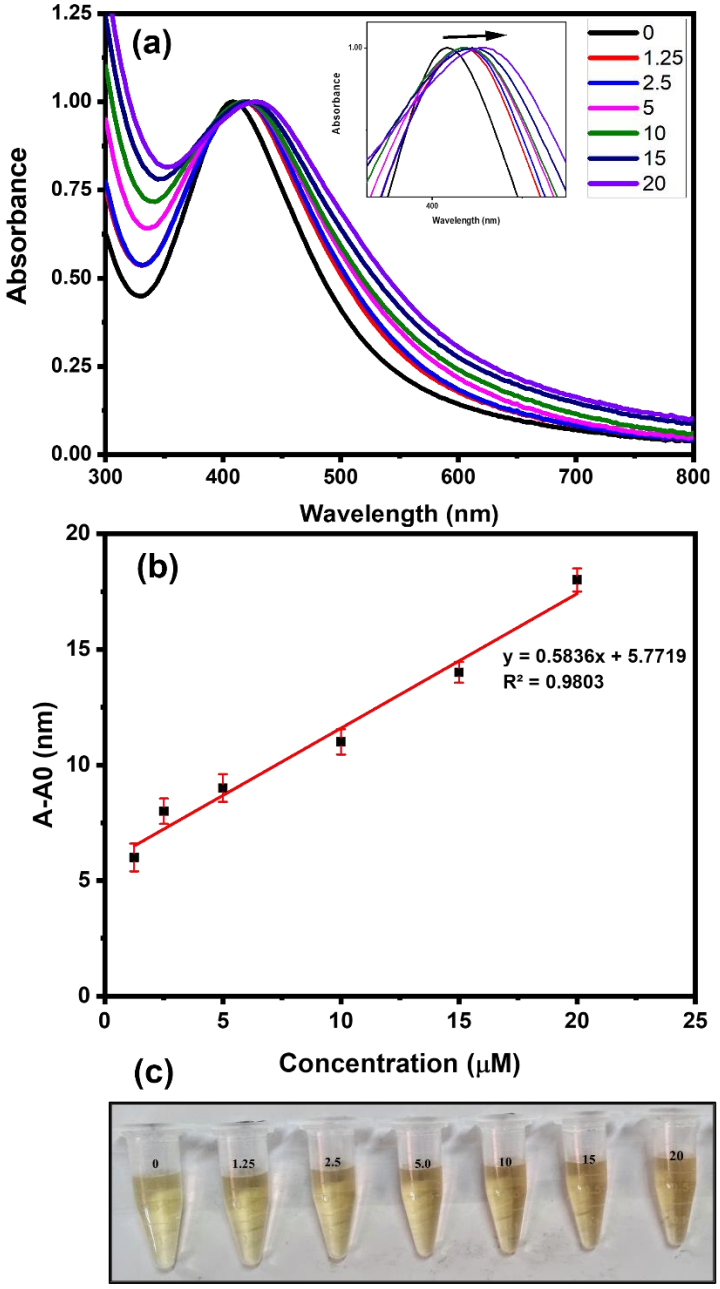

Figure 4.13: (a) UV-vis spectrum of Q-AgNPs having different concentration of L-Cys in urine solution (1.25-20 µM) (normalized spectra), inset wavelength shifting (b) Regression line displaying a red shift with respective L-Cys concentration (c) Colour change in Q-AgNPs at different L-Cys concentration in urine sample.

In addition, Q-AgNPs UV-visible spectrums at different L-Cys containing FBS solution also showed red shifts (Figure 4.14a), a maximal 22 nm red shift at 15 µM L-Cys concentration was observed. According to the linear regression equation, 230 nM LOD and 650 nM LOQ for L-Cys having FBS solution was recorded (Figure 4.14b). In Q-AgNPs solution treated with cysteine-containing FBS solution, significant colour changes brownish yellow from yellow were also noticed (Figure 4.14c).

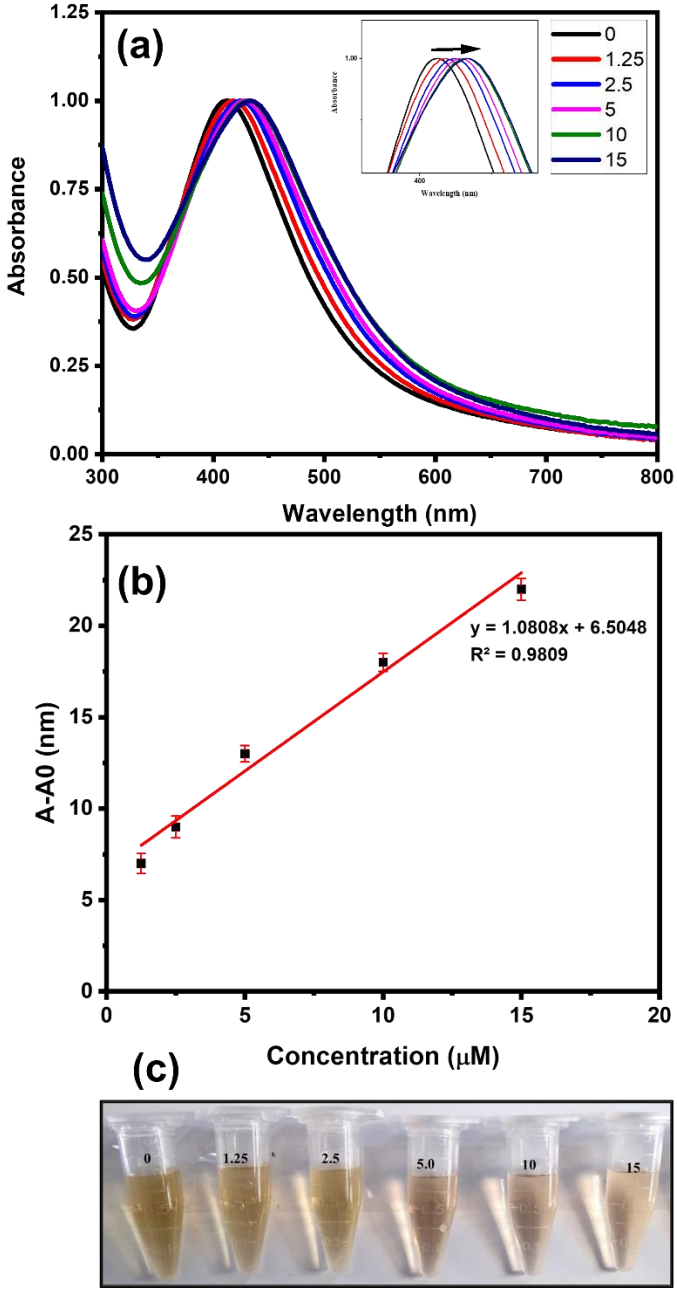

Figure 4.14: (a) UV-vis spectrum of Q-AgNPs having different concentration of L-Cys in FBS solution (1.25-15 µM) (normalized spectra), inset wavelength shifting (b) Regression line displaying a red shift with respective L-Cys concentration (c) Colour change in Q-AgNPs at different L-Cys concentration in urine sample.

Table 4.3 gives a comparison of earlier and present work that used various kind of nanoparticles to detect L-Cys. In terms of sensitivity, procedure convenience, and economic viability, Q-AgNPs as a sensor for L-Cys detection appear to be superior to the majority of existing research shown in Table 4.3. The current research suggests that Q-AgNPs have good sensing ability for the detection of L-Cys in biologically complex fluids at nM concentrations.

Table 4.3: Comparison of current research findings with existing research work.

Sr. No	Nanoparticle type	Method type	Range	Detection limit	Reference
1	AgNPs	Colorimetric	25-250 µM	20.63 µM	[462]
2	Fluorosurfactant-capped silver nanoparticles	Colorimetric	1.5-6.0 µM	0.05 µM	[428]
3	BAE/AgNPs	Colorimetric	0.05-1000 µM	0.035 µM	[412]
4	AgNPRs	Colorimetric	0.05-500 µM	0.01 µM	[405]
5	McAgNPs	Colorimetric	0.1-200 µM	0.043 µM	[245]
6	Silver nanoparticles	Colorimetric	0.1-10 µM	0.1 µM	[463]
7	Dios-AgNPs	Colorimetric	0-100 µM	0.0077 µM	[464]
8	Ag NPs	Colorimetric	0.1-1000 µM	0.1 µM	[465]
9	Dextran coated AgNPs	Colorimetric	100µM-1 mM	12 µM	[466]
10	AgNPs	Colorimetric	0.5-10 µM	0.068 µM	[467]
11	AgNPs	Colorimetric	0-60 µM	50 µM	[468]
12	3,3',5,5' tetramethylbenzidine	Colorimetric	4-290 µM	2.46 µM	[469]
13	S, N-doped carbon quantum dots	Fluorescent	10-120 µM	0.35 µM	[470]
14	Ag NCs and carbon dots	Fluorescent	20-80 µM	0.14 µM	[471]
15	TA based AuNPs	Colorimetric	0-990 µM	0.879 µM	[472]
16	Cu NCs	Fluorescent	5-50 µM	2.5 µM	[413]

17	DTNB-AuNPs	Colorimetric	0.4-29 µM	0.57 µM	[473]
18	Au-AgNPs	Fluorescent	2-100 µM	1.1 µM	[474]
19	Au-AgNCs	Fluorescent	200-600 µM	80 µM	[475]
20	Carbon Nanofiber electrode	Cyclic voltammetry	20-1000 µM	20 µM	[460]
21	DPP-AC	Fluorescent	0-70 µM	0.18 µM	[476]
22	Au-Ag NCs	Fluorescent	10-100 µM	2.5 µM	[477]
23	$CuMnO_2$ nanoflakes	Colorimetric	25-300 µM	11.26 µM	[478]
24	Cobalt-doped CDs	Fluorescent	0.1-100 µM	0.08 µM	[479]
25	**Q-AgNPs**	**Colorimetric**	**0.25-15 µM in water** **1.25-20 µM in urine** **1.25-15 µM in FBS**	**21.1 nM in water** **86 nM in urine,** **and 230 nM in FBS**	**Present Study**

4.4 SUMMARY

To summarize, we successfully established a single step method for synthesizing Q-AgNPs that seems to be environmentally benign, adaptable, and strong. The Q-AgNPs that were produced were spherical in morphology, with a mean size of around 40 nm. Furthermore, the synthesized Q-AgNPs were used for the detection of L-Cys in the aqueous and physiologically complex fluids like urine and FBS. Results revealed that Q-AgNPs upon exposure to aqueous, urine, and FBS solutions of L-Cys exhibits red shift of about 24 nm, 18 nm, and 22 nm respectively in the absorption band of Q-AgNPs. The changes were also prominent visually as there was significant change from yellow to brownish colour in the Q-AgNPs in all cases due to aggregation. Agglomeration of Q-AgNPs was believed to be caused by Ag-S interactions between the Ag of Q-AgNPs and thiol of L-Cys. The postulated mechanism was confirmed through SEM, TEM, and DLS investigation, which revealed that the presence of L-Cys leads to the Q-AgNPs agglomeration. The sensitivity analysis of Q-AgNPs for the detection of L-Cys revealed the detection limits of 21.1 nM (aqueous solution of L-Cys), 86 nM (urine solution of L-Cys), and 230 nM (FBS solution of L-Cys). The assessment of L-Cys sensitivity in complicated fluids was a maiden effort based on our knowledge of the literature. As a nutshell, our findings provide a straightforward, low-cost, and quick method for detecting cysteine in water, urine, and FBS solutions.

Chapter 4 presents work of 3rd and 4th objective. The work has been published in the journal ChemistrySelect (https://doi.org/10.1002/slct.202104147).

CONCLUSION, FUTURE PROSPECT, & NEW FINDINGS

Conclusion

The motive of current research work emphasized on synthesis of M-NP_S for treatment and diagnosis purposes using single step approach. In the present work we successfully synthesized gold and silver nanoparticles using one-pot approach. Gold nanoparticle were synthesized using a standard antibiotic for enhanced antibacterial potential. In addition to this, silver nanoparticles were also synthesized using flavonoid molecule for the sensing application. The synthesized M-NPs were characterized using various analytical and microscopic techniques to achieve information about their shape, size, and distribution.

Gentamicin is a standard antibiotic that has been generally recommended for the treatment of various infections. In the current piece of work, we have synthesized gold nanoparticles using gentamicin as reducing and stabilizing agent to produce gentamicin conjugated gold nanoparticles (G-AuNPs). G-AuNPs synthesis was achieved though one-pot approach. Ruby red colour appearance after mixing of optimized concentration of auric chloride and gentamicin initially highlighted the synthesis of G-AuNPs. However, G-AuNPs synthesis was evidenced by UV-vis spectroscopy through displaying absorption maxima of G-AuNPs at 520 nm. The TEM and DLS studies of G-AuNPs proposed that particles were approximately 15 nm in size with spherical morphology. Antibacterial activity of G-AuNPs revealed strong antibacterial potential of G-AuNPs against *E. fergusonii* ATCC 35469, *E. coli* ATCC 25922, *E. coli* DH5α, and *S. aureus* MTCC 3160 inhibitory zone of 14 mm, 15 mm, 11 mm, and 11 mm, respectively ($p>0.05$). The G-AuNPs were observed to had MIC of 0.0046 nM, 0.046 nM, 0.01 nM, and 0.0046 nM, ($p>0.05$) towards *S. aureus* MTCC 3160, *E. fergusonii* ATCC 35469, *E. coli* ATCC 25922, and *E. coli* DH5α, respectively. Antibacterial activity of G-AuNPs was due to the production of reactive oxygen species (ROS) and membrane lipid peroxidation (LPO) as evidenced by ROS and LPO estimation. Drug release analysis revealed that G-AuNPs released gentamicin in sustained manner with 53 % release in 72 h. The cytotoxicity analysis revealed that G-AuNPs were non-toxic to C2C12 cell line.

Simultaneously, we have synthesized silver nanoparticles (Q-AgNPs) using flavonoid molecule quercetin as reducing as well stabilizing agent. Various parameters like, reactants ratio, pH, and time were optimized to produce Q-AgNPs. The appearance of yellow colour in colourless solution of $AgNO_3$ (2 mM) after the addition of quercetin solution (50 µM), hints the synthesis of Q-AgNPs. The synthesis was confirmed by UV-vis spectroscopy, where Q-